

Electronic Supporting Information

Supramolecular Polymer-Assisted Synthesis of Nitrogen and Sulfur Dual-Doped Porous Graphene Networks from Petroleum Coke as Efficient Metal-Free Electrocatalysts for Oxygen Reduction Reaction

Mingbo Wu^{a*}, Yang Liu^a, Yulong Zhu^a, Jin Lin^c, Jingyan Liu^a, Han Hu^b, Yang Wang^a, Qingshan Zhao^a, Renqing Lv^c, Jieshan Qiu^{b*}

Supplementary data

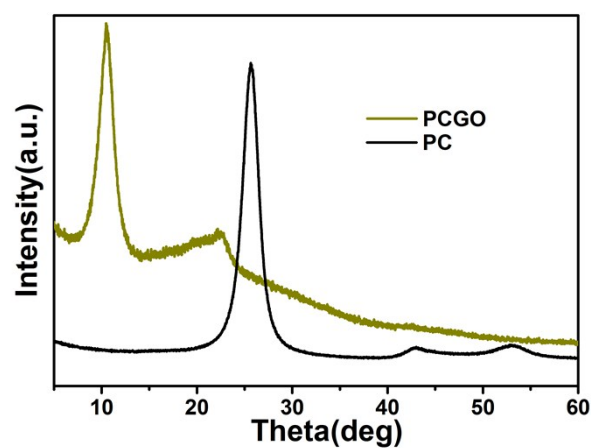


Figure S1. XRD patterns of PC and PCGO.

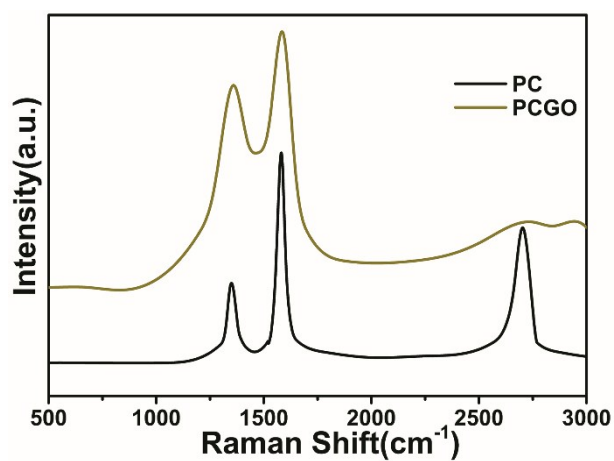


Figure S2. Raman spectra of PC and PCGO.

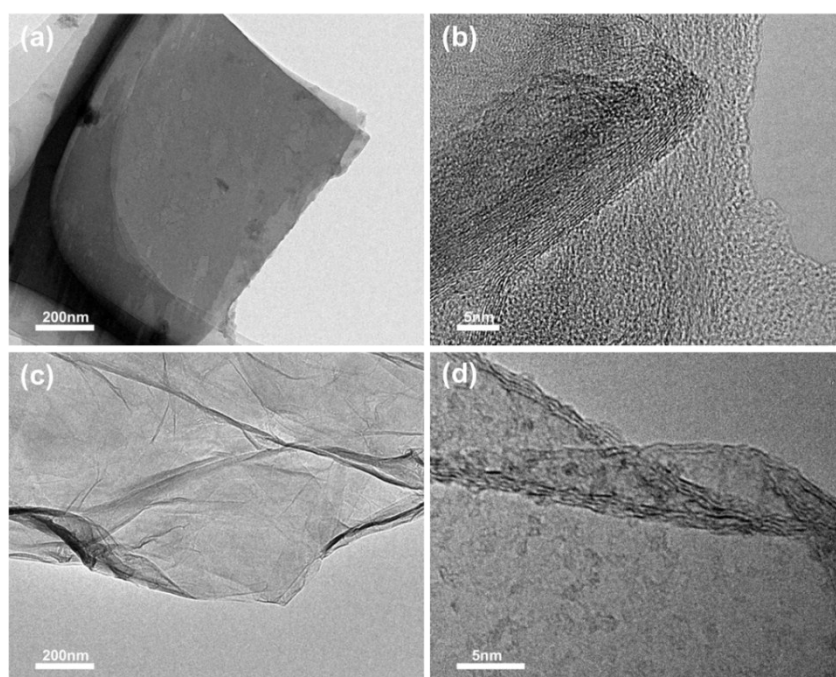


Figure S3. TEM and HRTEM images of (a, b) PC and (c, d) PCGO.

In the TEM and HETEM observation of the PCGO sheets, only three to five graphene layers were observed. No remarkable dark multilines corresponding to the graphene layers were found in a wide view field.

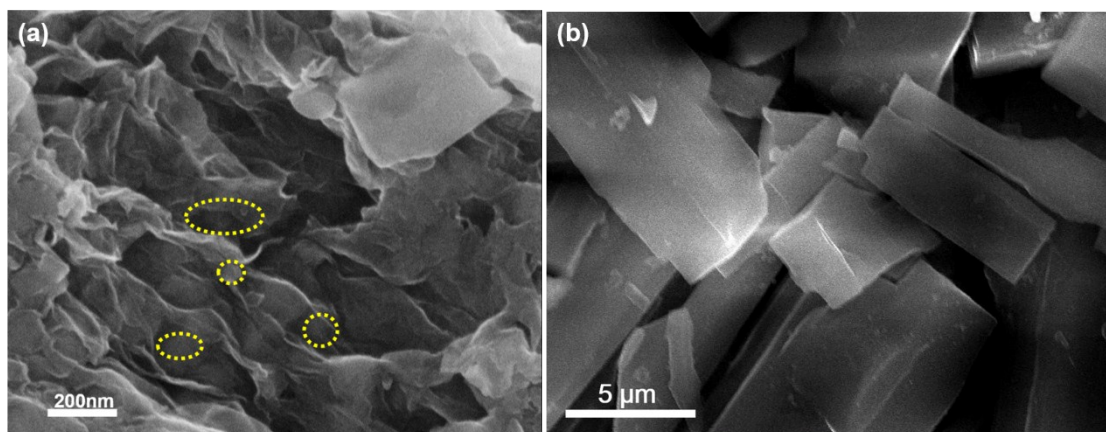


Figure S4. SEM images of (a) MT@GO from natural graphite and (b) MT obtained under same condition without PCGO.

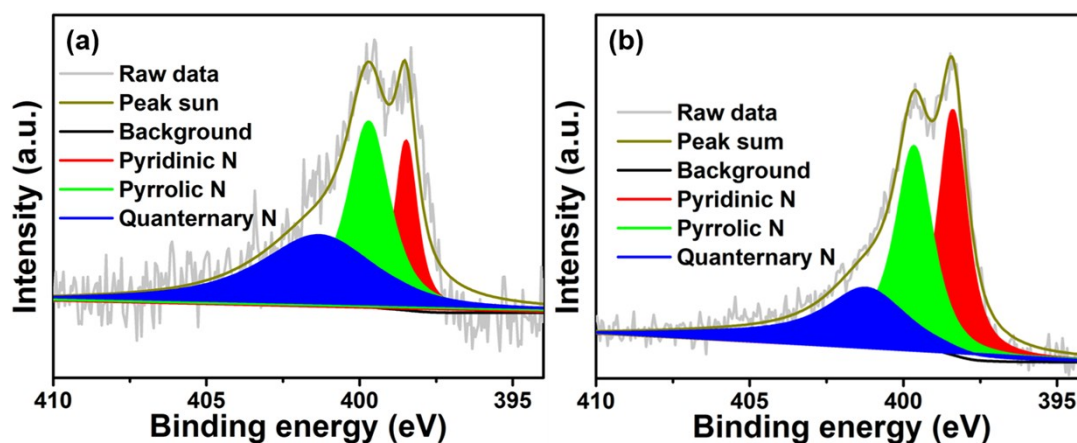


Figure S5. High resolution N1s spectra of (a) N,S-PGN-700 and (b) N,S-PGN-900.

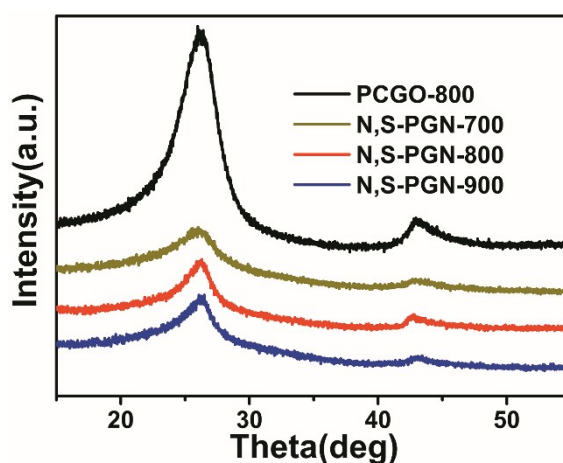


Figure S6. XRD patterns of N,S-PGNs and PCGO-800.

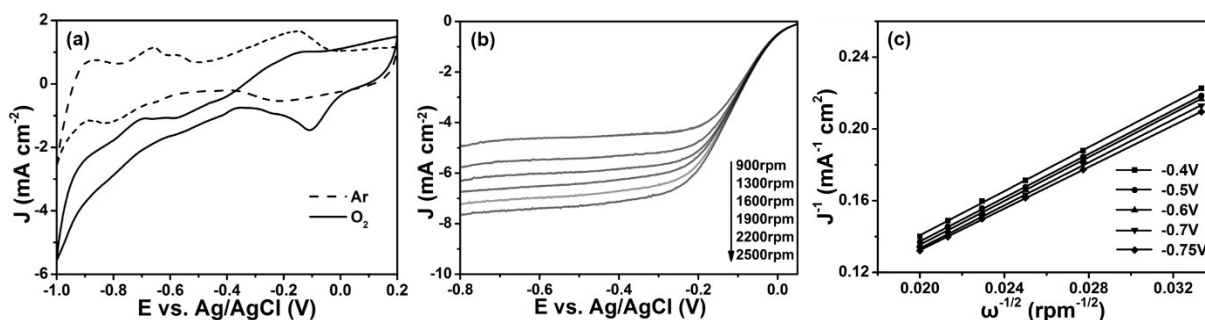


Figure S7. (a) CV curves of Pt/C in Ar and O₂ saturated 0.1M KOH aqueous solution with a scan rate of 10 mV s⁻¹. (b) LSV curves of Pt/C at different rotating speeds. (c) Koutecky-Levich plots at different potentials based on the results of (b).

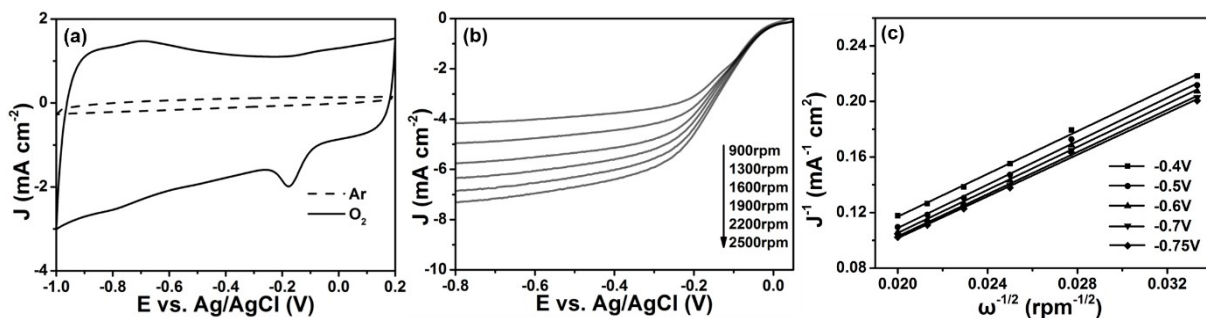


Figure S8. (a) CV curves of N,S-PGN-700 in Ar and O₂ saturated 0.1M KOH aqueous solution with a scan rate of 10 mV s⁻¹. (b) LSV curves of N,S-PGN-700 at different rotating speeds. (c) Koutecky-Levich plots at different potentials based on the results of (b).

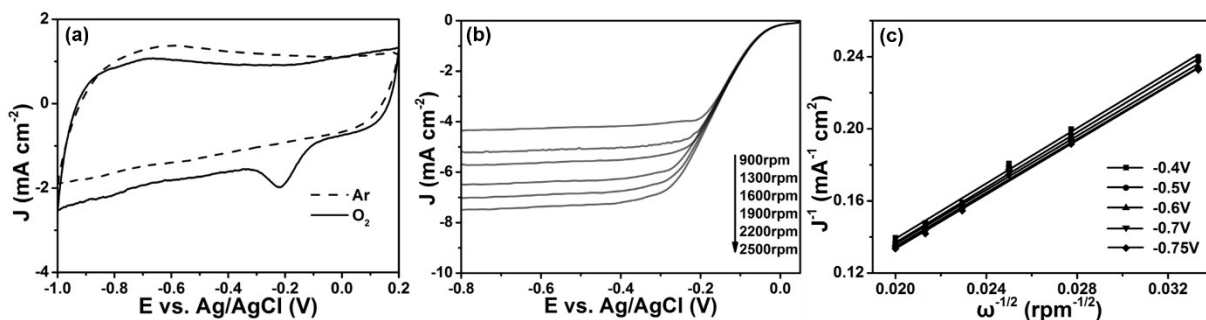


Figure S9. (a) CV curves of N,S-PGN-900 in Ar and O₂ saturated 0.1M KOH aqueous solution with a scan rate of 10 mV s⁻¹. (b) LSV curves of N,S-PGN-900 at different rotating speeds. (c) Koutecky-Levich plots at different potentials based on the results of (b).

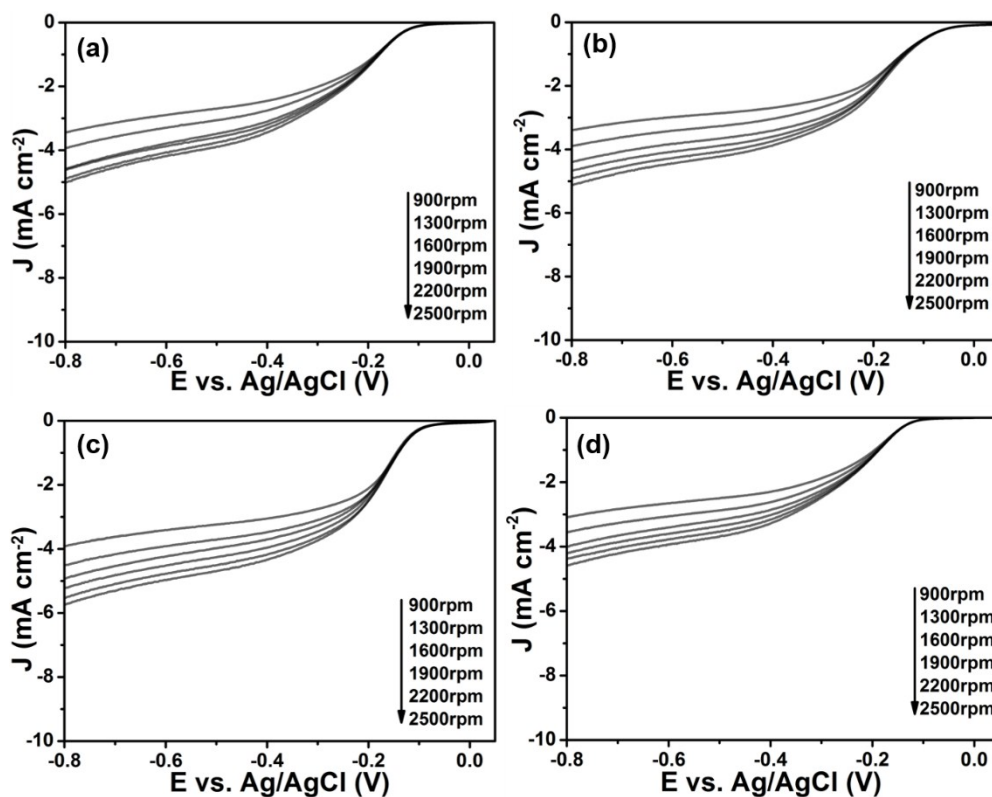


Figure S10. LSV curves of (a) PCGO-800, (b) N,S-G-800, (c) M-G-800 and (d) T-G-800 at different rotating speeds.

As can be seen, the other referential carbon catalysts exhibit inferior ORR catalytic performances compared to N,S-PGNs, indicating that not only the charge density on active centers can be improved by co-doping, but also the edge-induced defects can be increased due to the unique porous architecture, resulting in the remarkable electrochemical performances of N,S-PGN.

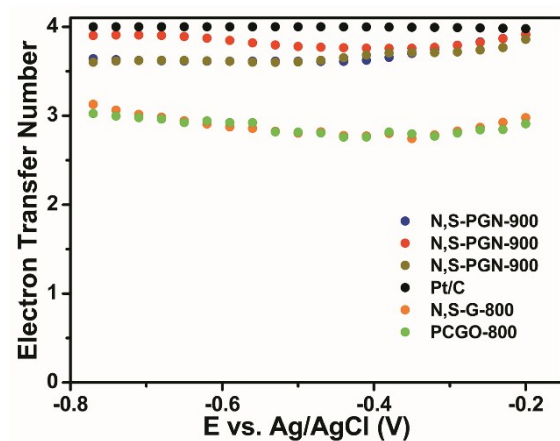


Figure S11. Electron transfer number (n) derived from the LSV curves in RRDE measurements.

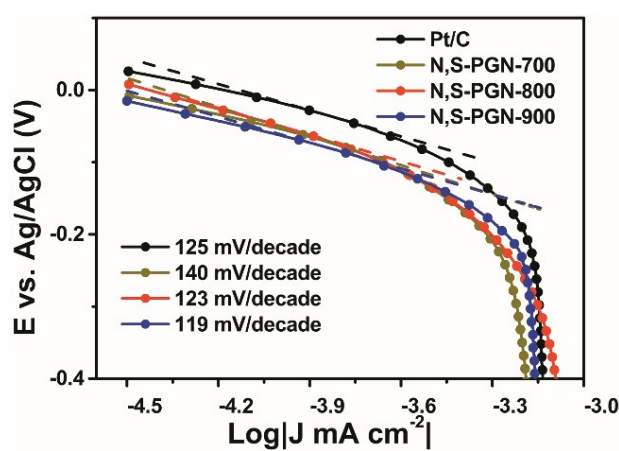


Figure S12. Tafel plots of N,S-PGNs and Pt/C.

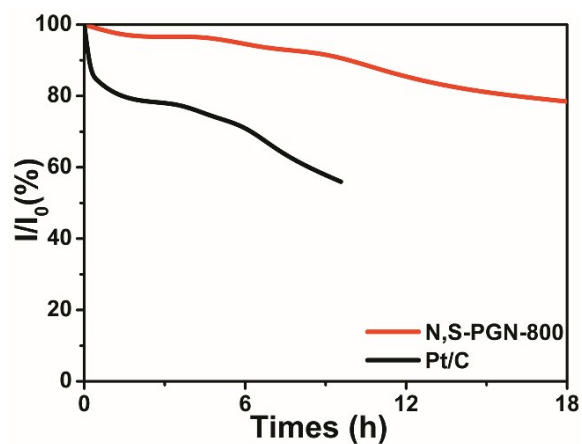
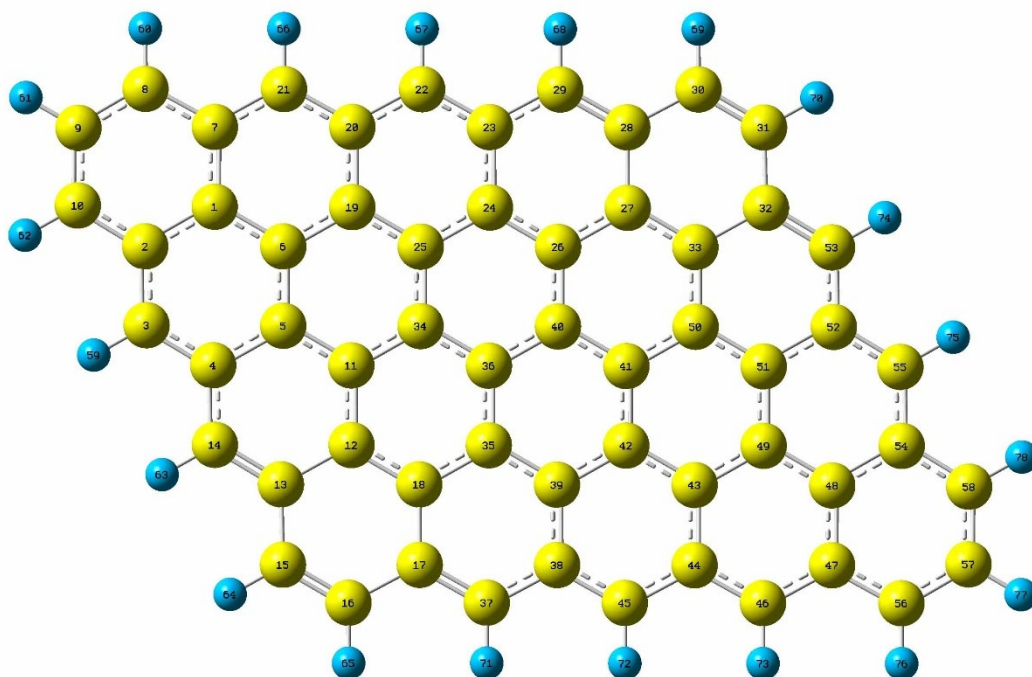


Figure S13. ORR chronoamperometric responses of N,S-PGN-800 and Pt/C at -0.4 V vs. Ag/AgCl with a rotation speed of 1600 rpm for 18 h.

(a)



(b)

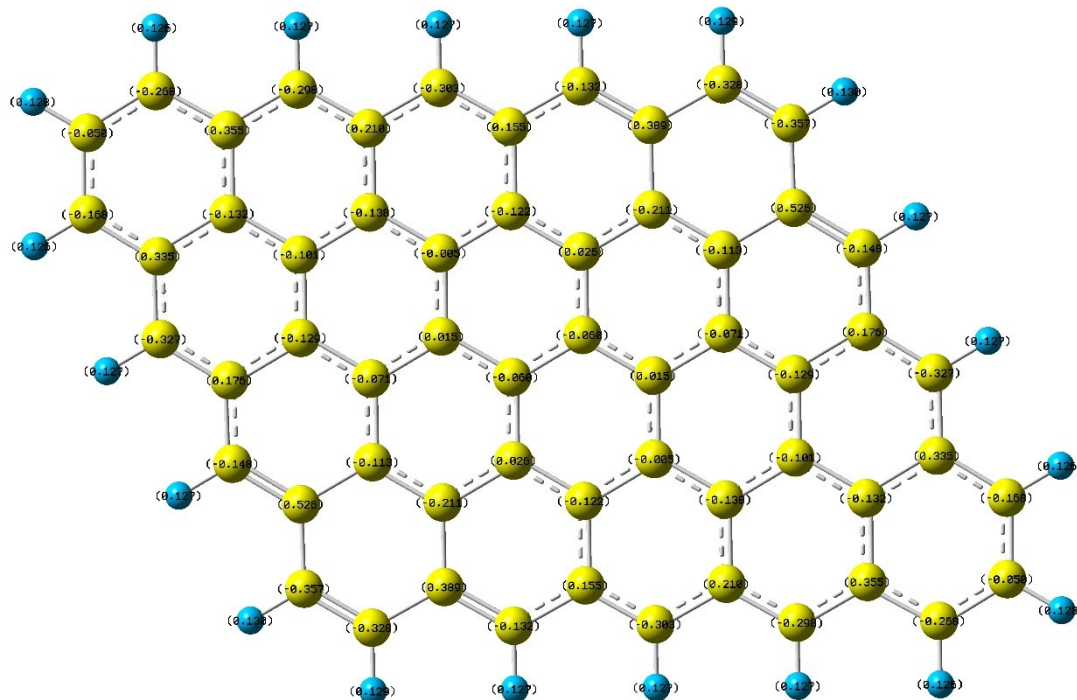
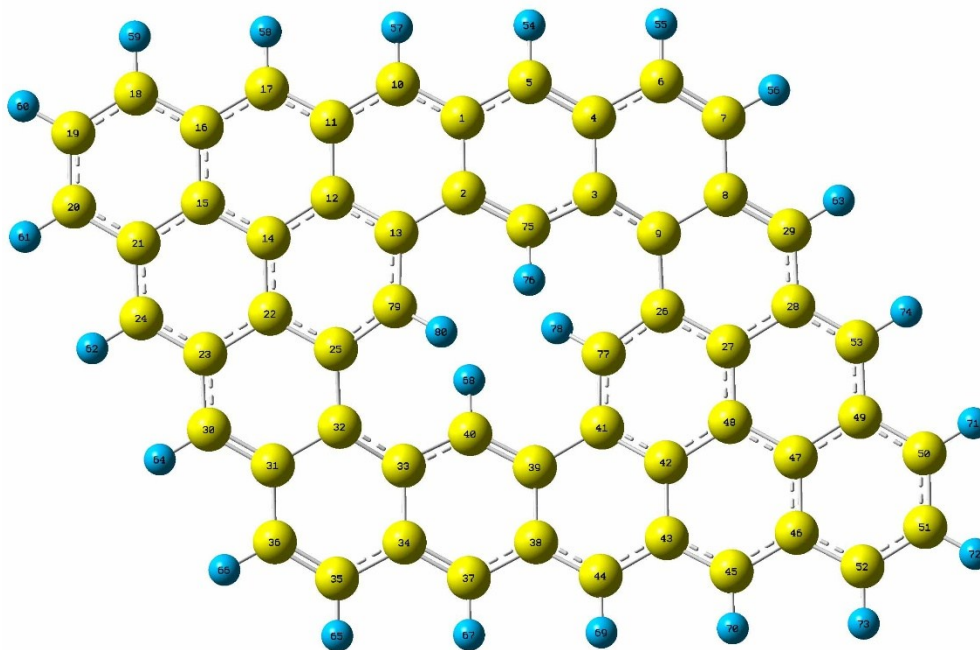


Figure S14. (a) Atomic order and (b) Mulliken charges distribution on pristine graphene models. Yellow and sky-blue are carbon and hydrogen, respectively.

(a)



(b)

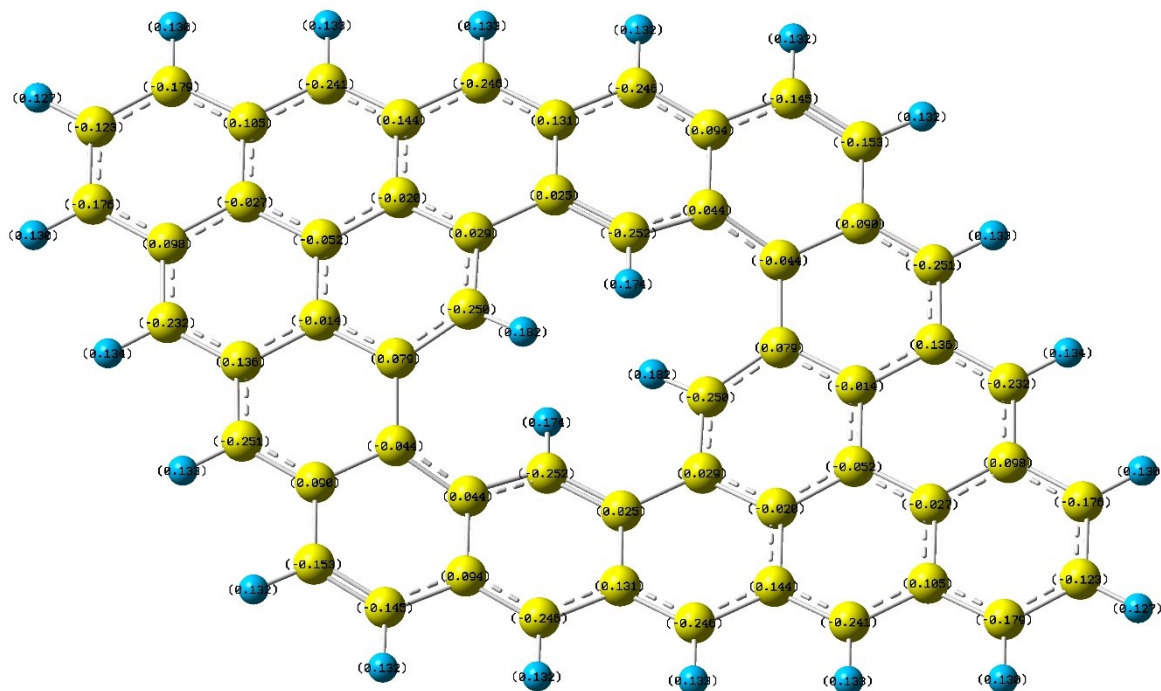
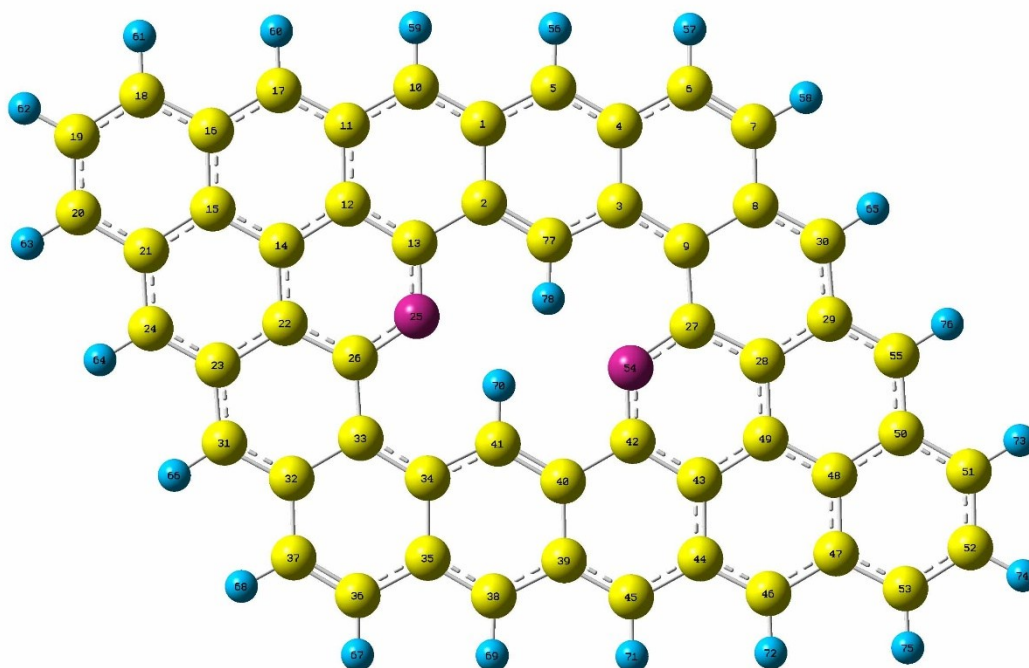


Figure S15. (a) Atomic order and (b) Mulliken charges distribution on porous graphene models. Yellow and sky-blue are carbon and hydrogen, respectively.

(a)



(b)

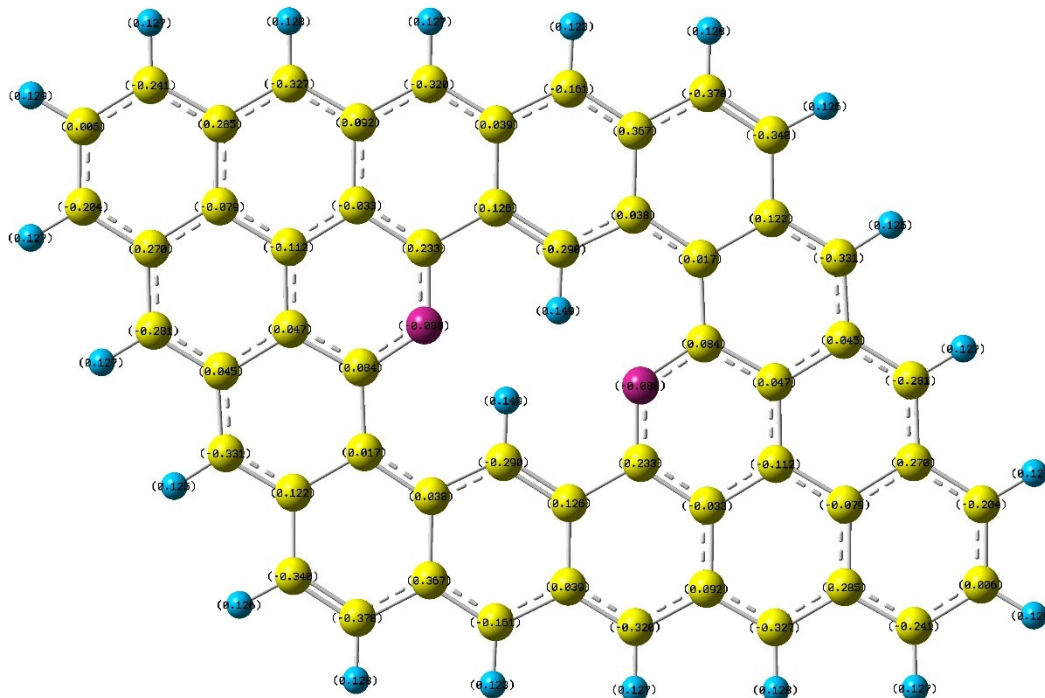
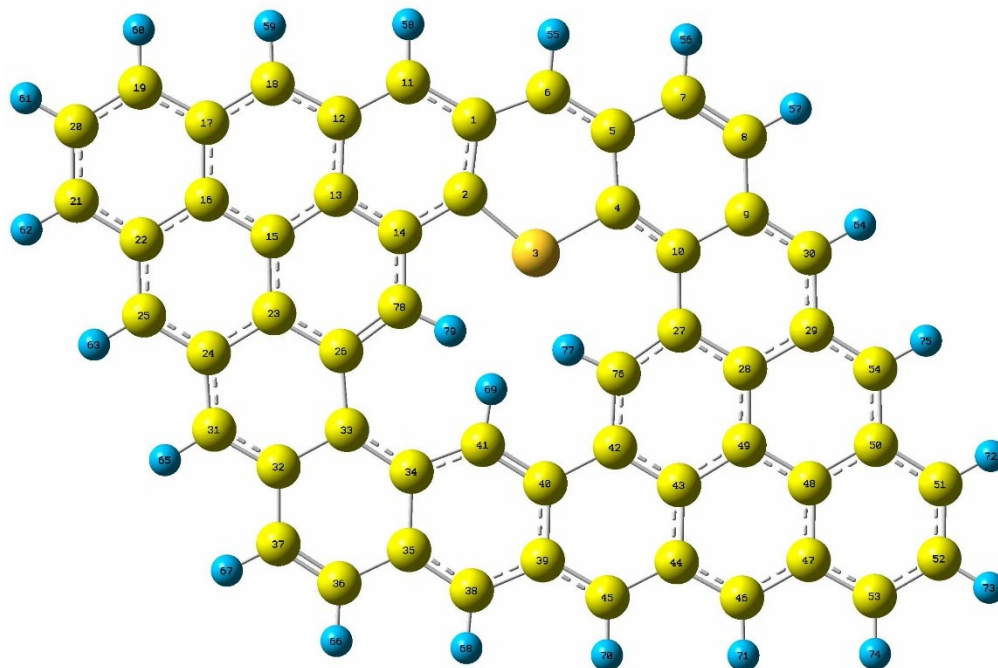


Figure S16. (a) Atomic order and (b) Mulliken charges distribution on N-doped porous graphene networks (N-PGN) model. Yellow is carbon, sky-blue is hydrogen, and purple is nitrogen.

(a)



(b)

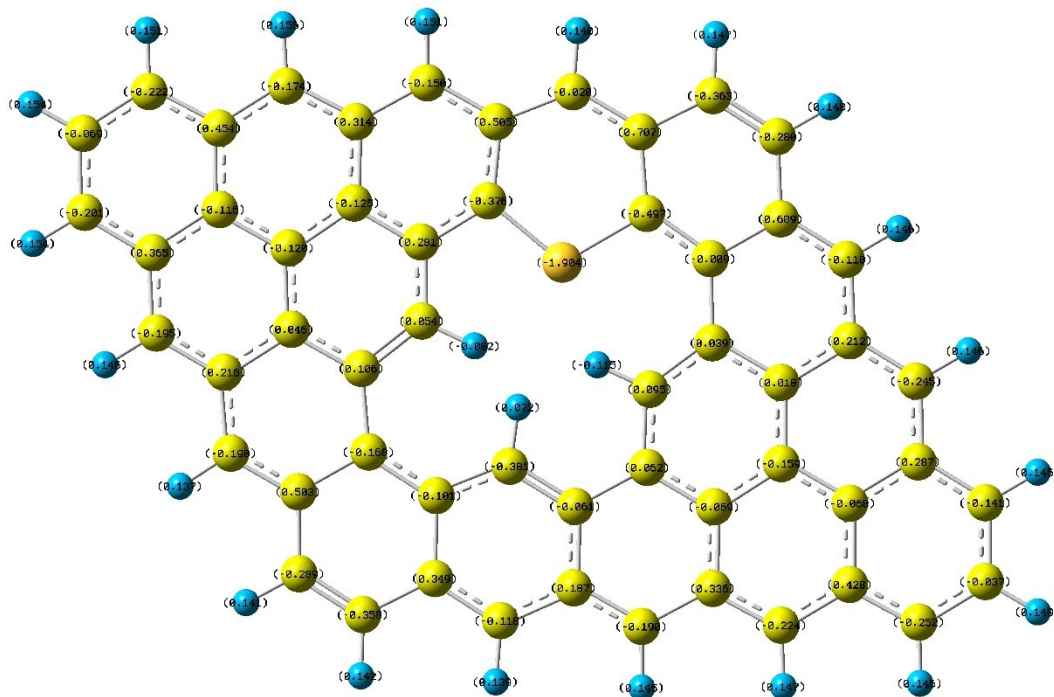


Figure S17. (a) Atomic order and (b) Mulliken charges distributions on S-doped porous graphene networks (S-PGN) model. Yellow is carbon, sky-blue is hydrogen, and orange is sulfur.

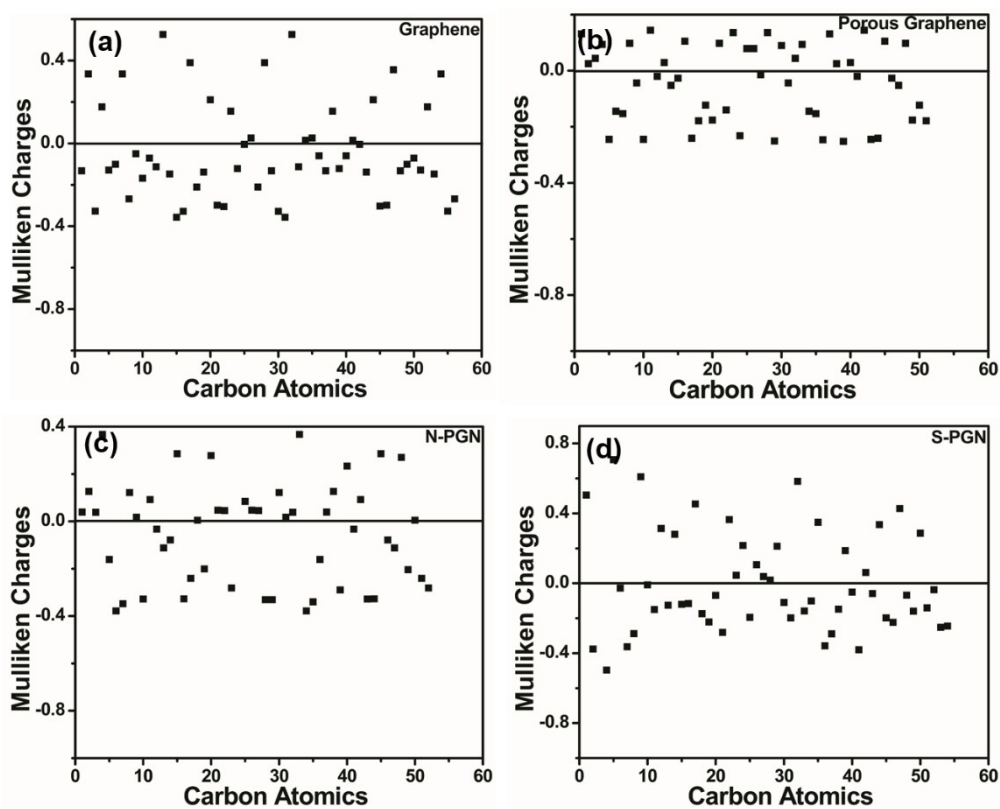


Figure S18. Mulliken charges of carbon atoms in (a) pristine graphene, (b) porous graphene, (c) N-PGN and (d) S-PGN.

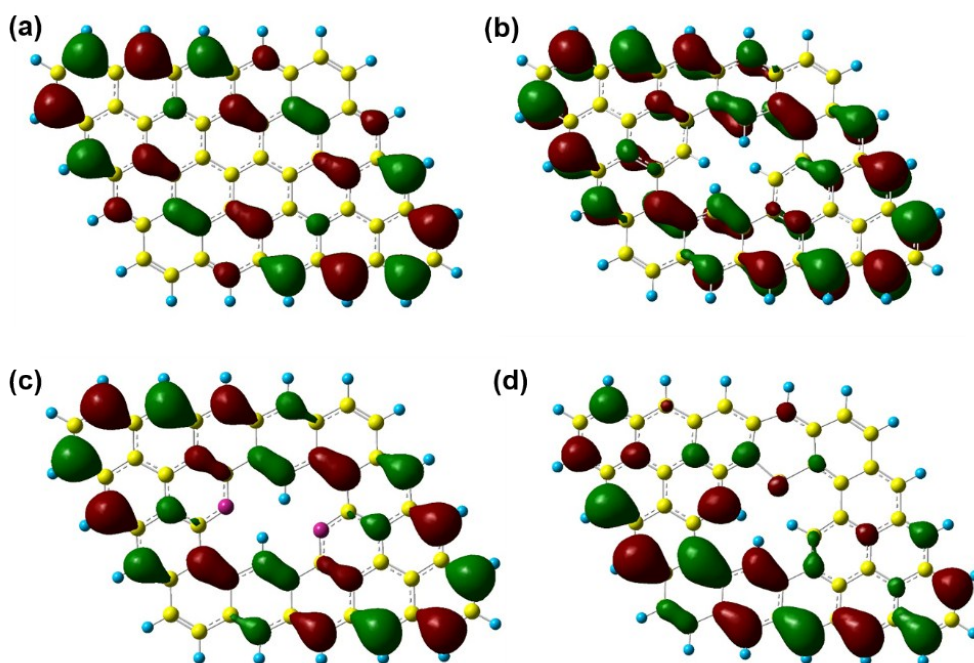


Figure S19. HOMO distributions on (a) pristine graphene, (b) porous graphene, (c) N-PGN and (d) S-PGN.

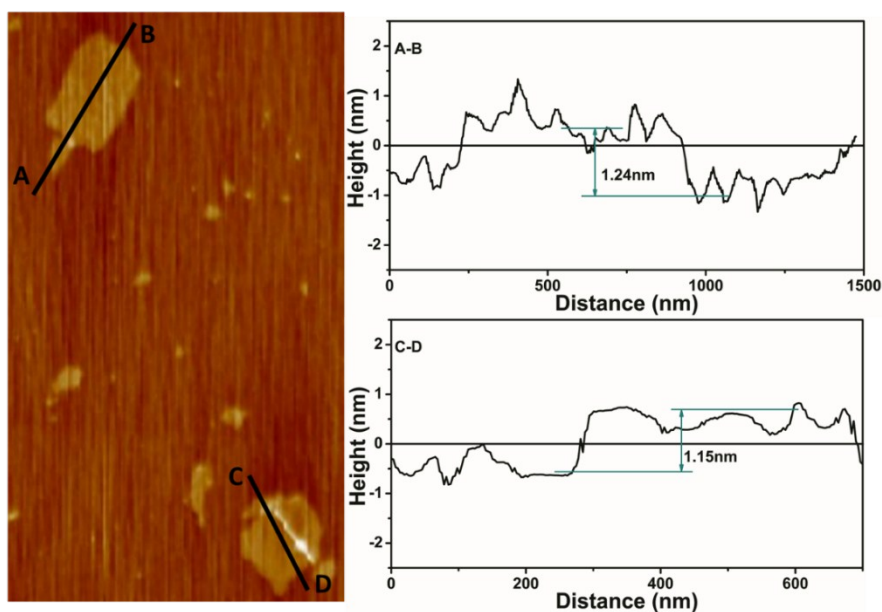


Figure S20. Atomic force microscope (AFM) photos and height profile of PCGO.

As shown, the thickness of PCGO sheet is ~ 1.2 nm, indicating that it contains no more than five graphene layers, which is consistent with TEM and HETEM results. It is believed that the characteristics discussed above prove the rationality of oxidizing method developed to produce PCGO from PC.¹⁻³

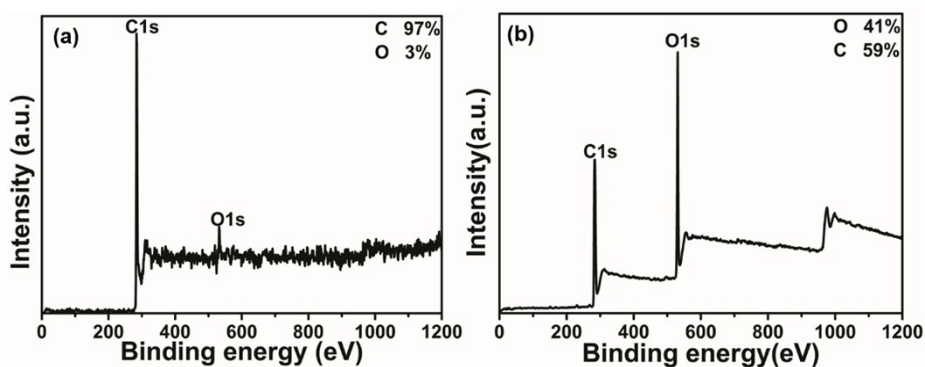


Figure S21. XPS survey spectra of (a) PC and (b) PCGO.

As can be seen, PCGO possesses higher oxygen content compared with PC and without any other metal elements, indicating the efficient introduction of oxygen-containing functional groups, and the reliability of oxidizing method developed from PC to PCGO.

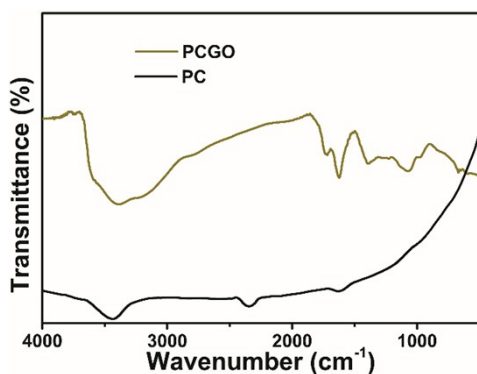


Figure S22. FTIR spectra of PC and PCGO.

As shown in Figure S21, it is observed that PCGO exhibits characteristic absorption peaks originated from C=O stretching vibration of carboxyl groups (1735 cm^{-1}), C=C stretching vibration of graphitic domains (1629 cm^{-1}), O-H stretching vibration (1224 cm^{-1}), and C-O stretching vibration from epoxy or alkoxy groups (1058 cm^{-1}).²⁻⁴

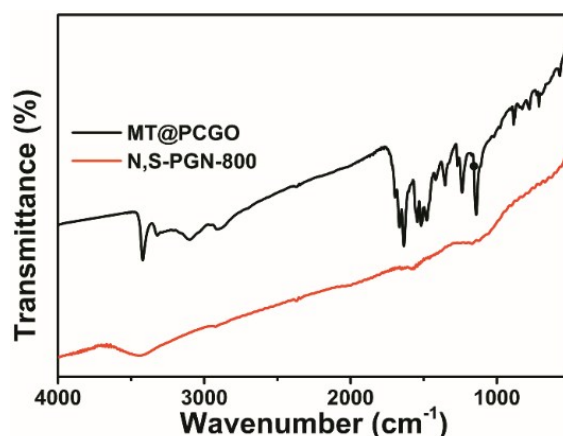


Figure S23. FTIR spectra of MT@PCGO and N,S-PGN-800.

In the FTIR spectrum of MT@PCGO, peaks located at 500-1600 cm^{-1} belong to vibrations of C-O, C-S, and C-C groups in MT and PCGO. After annealing at 800 $^{\circ}\text{C}$ in N_2 atmosphere, N,S-PGN demonstrates a featureless FTIR spectrum except for some weak peaks originated from the stretching vibration of O-H (3400 cm^{-1}), C=C (1629 cm^{-1}), C-S (1150 cm^{-1}) and C-O (1028 cm^{-1}) groups, indicating the successful doping of heteroatoms generated from MT.^{4,5}

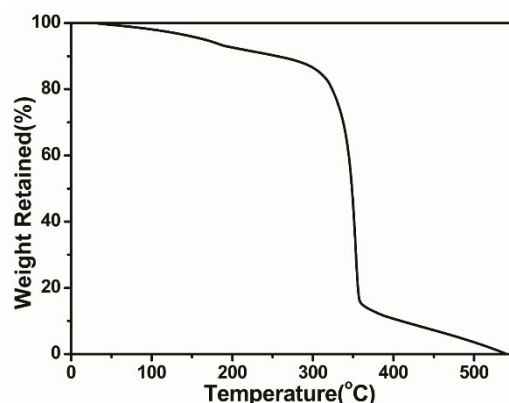


Figure S24. TGA profile of MT measured from 30 to 600 $^{\circ}\text{C}$ at a heating rate of $10 \text{ }^{\circ}\text{C min}^{-1}$ in N_2 .

The TGA in N_2 has been showed that the weight loss of MT reached 100% at about 540 $^{\circ}\text{C}$, indicating that has no MT (or S-doped C_3N_4 or carbon) residues after calcination for 2 h at 700 $^{\circ}\text{C}$ let alone higher temperature (800 and 900 $^{\circ}\text{C}$).

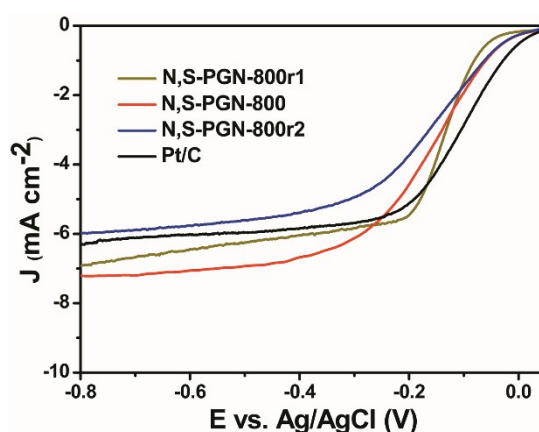


Figure S25. LSV curves of N,S-PGN-800, N,S-PGN-800r1, N,S-PGN-800r2 and Pt/C in O_2 -saturated 0.1 M KOH electrolyte with a 5 mV s^{-1} and a rotation rate of 1600 rpm.

Although the contents of N and S were not a highest-level, N,S-PGN-800 possess the best electrochemical performance comparing with the N,S-PGN-800r1 and N,S-PGN-800r2. Combined with the results showed in Table S1, we can draw a conclusion that N and S doping rate in N,S-PGN was not a only factor to improve the ORR performance.

Table S1. Elemental composition and electrocatalytic performance of N,S-PGNs, PCGO-800 and N,S-G-800.

| Samples | N content (at.%) | S content (at.%) | I_D/I_G | ΔE_{onset} (mV) ^{a)} | $E_{1/2}$ (V) | J_L (mA cm ⁻²) | n |
|---------------|------------------|------------------|-----------|--|---------------|------------------------------|---------|
| PCGO-800 | – | – | 0.65 | -125 | -0.29 | -4.4 | 2.7-3.2 |
| N,S-G-800 | 6.5 | 1.1 | 0.81 | -50 | -0.214 | -4.6 | 2.7-3.1 |
| N,S-PGN-700 | 12.5 | 1.9 | 1.03 | -10 | -0.149 | -5.8 | 3.5-3.6 |
| N,S-PGN-800 | 9.7 | 1.6 | 1.15 | -10 | -0.155 | -7.2 | 3.9-4.0 |
| N,S-PGN-900 | 7.1 | 1.1 | 1.05 | -11 | -0.147 | -5.7 | 3.5-3.9 |
| N,S-PGN-800r1 | 5.6 | 1.4 | – | -10 | -0.165 | -6.0 | 3.5-3.9 |
| N,S-PGN-800r2 | 10.7 | 1.7 | – | -30 | -0.145 | -6.9 | 3.7-4.0 |

$$^a) \Delta E_{\text{onset}} = E_{\text{onset}}(\text{Samples}) - E_{\text{onset}}(\text{Pt/C})$$

Table S2. Comparison of the electrocatalytic performance of N,S-PGN-800 and other metal-free electrocatalysts toward ORR.

| Catalysts | Catalyst loading (mg cm ⁻²) | ΔE_{onset} (mV) ^{a)} | $\Delta E_{1/2}$ (mV) ^{b)} | J_L (mA cm ⁻²) | n | Ref. |
|---------------------------------------|---|--|-------------------------------------|------------------------------|-----------|--|
| Meso/micro-PoPD | 0.5 | -30 | 0 | 4.32 | 2.62-3.86 | <i>Nat. Commun.</i> , 2014, 4973 , 1. |
| N-doped nanoporous carbon nanosheets | 0.1 | -85 | -105 | ~4.5 | 3.7-4.0 | <i>Energy Environ. Sci.</i> , 2014, 7 , 4095. |
| NGM | 0.25 | -50 | -30 | 6.41 | 3.8 | <i>Adv. Mater.</i> , 2016, 28 , 6845. |
| N,S-codoped carbon nanosheets | 0.3 | -50 | -50 | ~4.6 | 3.89-4.0 | <i>Nano Energy.</i> , 2016, 19 , 373. |
| N,S-co-doped porous carbon nanosheets | 0.25 | -40 | -27 | ~4.8 | 3.9 | <i>Adv. Funct. Mater.</i> , 2016, 26 , 5893. |
| Pt/C | 0.3 | 0 | 0 | 6.4 | 3.9-4.0 | this work |
| N,S-PGN-800 | 0.3 | -10 | -30 | 7.2 | 3.9-4.0 | this work |

$$^a) \Delta E_{\text{onset}} = E_{\text{onset}}(\text{Catalysts}) - E_{\text{onset}}(\text{Pt/C}); \quad ^b) \Delta E_{1/2} = E_{1/2}(\text{Catalysts}) - E_{1/2}(\text{Pt/C})$$

References

- 1 L. Peng, Z. Xu, Z. Liu, Y. Y. Wei, H. Y. Sun, Z. Li, X. L. Zhao and C. Gao, *Nat. Commun.*, 2015, **5716**, 1.
- 2 Y. X. Xu, H. Bai, G. W. Lu, C. Li and G. Q. Shi, *J. Am. Chem. Soc.*, 2008, **130**, 5856.
- 3 H. Hu, Z. B. Zhao, Q. Zhou, Y. Gogotsi and J. S. Qiu, *Carbon*, 2012, **50**, 3267.
- 4 N. P. Wickramaratne, V. S. Perera, J. M. Ralph, S. D. Huang and M. Jaroniec, *Langmuir*, 2013, **29**, 4032.
- 5 W. T. Wu, G. L. He, T. Chen, C. X. Guo, Z. S. Lu, J. N. Selvaraj, Y. Liu and C. M. Li, *Chem. Commun.*, 2014, **50**, 21335.